UNIVERSITY OF WEST ATTICA

eISSN:3136-7658

Applied Manufacturing Intelligence Journal

Vol. 5, No. 3, July, 2026



Rubber Seal Deformation Measurement with a Causality-Enhanced S4D-Mixer Prediction Model

Dimas Firmansyah[1,*], Luthfi Ramadhan[1]

[1] *Department of Artificial Intelligence, Faculty of Informatics, Universitas Telkom, Bandung, 40257, Indonesia*

Received 24 May 2026; Revised 05 September 2026; Accepted 09 September 2026; Published 12 September 2026

Abstract

Rubber seal deformation measurement is required for assembly quality inspection because seal compression, edge displacement and recovery behavior determine pressure-bearing capacity and long-term sealing performance. This paper introduces a causality-enhanced S4D-Mixer prediction model for deformation measurement of rubber sealing rings based on visual and mechanical data. Seal images, edge-offset features, compression displacement, load response, fixture position and image-quality indicators are aligned into a deformation window. The S4D branch models ordered loading, holding and recovery changes, while the Mixer branch fuses image and mechanical variables without relying on a single local texture cue. A causal regularisation module is introduced to distinguish real deformation evidence from unstable associations caused by lighting variation, fixture displacement or reflective rubber surfaces. The simulated experiments include normal compression, under-compression, over-compression, eccentric compression and edge-folded states, and the production-style dataset contains 5,280 measurement windows. The proposed model achieves a mean absolute deformation error of 0.043 mm and 91.8% high-risk deformation recall, while reducing false alarms caused by reflective surfaces compared with convolutional and recurrent baselines. The output includes predicted deformation, confidence score, dominant evidence and review priority. This structure supports high-speed seal screening, measurement traceability and maintenance inspection for automated rubber-component assembly lines.

Keywords: Rubber Seal Deformation; Causality-Enhanced Prediction; S4D-Mixer Model; Industrial Measurement; Quality Inspection

1. Introduction

Rubber sealing rings are widely used in fluid equipment, automotive assemblies and precision mechanical joints because elastomeric compression can compensate for machining clearance [1]. Deformation measurement is a core quality-control task because insufficient compression may cause leakage, whereas excessive compression may accelerate material fatigue [2]. Visual inspection is useful for observing edge distortion and fold formation, but rubber surfaces often show weak texture and high reflectance [3]. Load-displacement sensing can describe compression response, although it cannot directly locate local edge deformation or asymmetric contact [4]. These complementary sources make seal inspection a multi-source measurement problem rather than a simple appearance-classification task. A production line needs to determine not only whether a seal is present, but also whether the shape, compression position and recovery state remain within the allowable process range.

The typical measurement equipment are hand-calipers, profile projectors, machine-vision contour extractors and load-bearing compression testing devices. Manual inspection is flexible but relatively slow and subject to the operator's judgment. Profile projection is accurate for the selected cross-sections, but it is not possible to connect the

* Corresponding author: dimas.fir92@telkomuniversity.ac.id

https://doi.org/10.68406/amij.2026.vol5iss3np7:94-106

➢ This is an open access article under the CC BY-NC-SA 4.0 license (https://creativecommons.org/licenses/by/4.0/).

© Authors retain all copyrights.

measured section with the whole ring under dynamic compression. Machine-vision technology can locate the outer and inner edges of a sealing ring; however, if the surface of the rubber is dark, glossy or partially covered, the results will be unreliable. Recent industrial quality research [5] has shown that visual measurement systems should also incorporate data-quality assessment in their application to production environments. A mechanical structure is required, and since the two rings have the same-shaped edges but will respond differently to the same compression, this structure will be used.

Deep learning has advanced industrial measurement by learning features from image sequences and sensor data. Convolutional networks can learn local edge deformations, and recurrent networks can model compression history. State-space sequence models [6] are relatively simple to use for modelling long windows, and they do not need to pay attention to all the frames. Mixer-type architectures [7] are also suitable for structured industrial data and integrate channel information and token information under fewer assumptions of spatial locality. The measurement problem in automated assembly is further exacerbated by the need to inspect the sealing ring at various stages of movement, pressing and release. Recently, studies on automated inspection [8] have shown that inspection systems for deformable parts need to keep both the process status and visual evidence. Research on quality prediction [9] has also shown that the production model should not assume all samples are from a fixed distribution. Robust industrial learning studies [10] have shown that the models employed in manufacturing need to suppress unstable shortcuts; therefore, the proposed model focuses on causal evidence from edge displacement, load residual and rebound behaviour, and utilizes image quality as a reliability signal.

A causality-enhanced S4D-Mixer model for rubber seal deformation measurement is presented in this paper. Section 2 reviews rubber component quality measurement, state-space and Mixer models, and causal evidence for industrial prediction. Section 3 builds the deformation evidence representation, S4D-Mixer prediction backbone, causal regularisation and output design. Section 4 evaluates prediction accuracy, generalisation, causal interpretability and inspection decisions using simulated production data. Section 5 summarizes the main findings, deployment limitations and future validation requirements for automated seal-inspection lines.

2. Related Work

2.1. Rubber Component Quality Measurement

Quality assessment of rubber components differs from rigid-part inspection due to the deformation of a rubber seal under load, its recovery upon release, and delayed shape recovery. Optics are employed for the measurement of outer diameter, inner diameter, end-to-end displacement, and surface defects. A Contact Sensor Measures Compression Distance, Force Response and Rebound Displacement. Research on manufacturing inspection [11] has found that for flexible components, both geometric and mechanical indicators are required, as the final quality state is affected by a combination of shape and load. Sealing rings are relatively tolerant of small edge deviations at a low pressure, but they are easily damaged by high compression or eccentric clamping.

The problem is that deformation is not always caused by a change in shape. The seal may have a small fold, an edge roll, non-uniform bulging or incomplete rebound. The above patterns may be mistaken for image noise, mould marks or surface reflections. Recent visual inspection studies [12] have shown that image-quality variation can lead to false defect detection of dark industrial materials. Therefore, the measurement model should keep the indicators of image quality and load-state variables, but it should not assume that the image is sufficient evidence. Research has shown that in a seal-inspection model, visual deformation is related to mechanical inconsistency.

Seal deformation also depends on boundary constraints during assembly. Uniform compression, off-centre pressure or a trap-and-hold device for the ring can be employed. Recently, manufacturing metrology research has investigated how to distinguish between intentional compression and unintentional local displacement in deformation measurement [13]. The two types of adjustment are not the same; therefore, a load-control device needs to be added to maintain evenness of over-compression, and eccentric deformation requires fixture alignment.

2.2. State-Space and Mixer Models

Sequence model is suitable because seal deformation occurs at the time of loading, holding and unloading. Recurrent Neural Networks can learn short-term dependencies, but the information of distant events in sequences with many stable frames may be lost in the hidden state. Transformers can address the problem of long-distance dependencies but are relatively complex. Structured State-Space Models [14] are well-suited for long-sequence modeling and express temporal changes through state updates. This characteristic is suitable for measuring compression because the model needs to remember the early-loading behaviour during observation of the later-recovery response.

Mixer-style models are used to reorganize features across tokens and channels. The variables of image edge offset, compression load, displacement residual and fixture state in industrial measurement are not independent. Bulgakov et al. [15] found that feature-embedding and interaction models can improve prediction performance when each variable has a different engineering meaning under different operating conditions. Seal deformation may be caused by actual compression, fixture eccentricity or camera-angle offset near the edge. Therefore, a Mixer module can combine local image features and mechanical parameters into a compact representation for deformation prediction.

Image-based deformation measurement therefore needs to be linked to process variables. If only the contour image is used, it is difficult to determine whether the edge shift is caused by compression depth, camera angle or ring misalignment. Oliveira et al. [16] showed that explainable defect-detection models can improve industrial inspection traceability by linking prediction results with evidence sources. In this study, the predicted deformation is therefore accompanied by the main evidence source, so that engineers can identify whether the result is mainly supported by image evidence, mechanical evidence or measurement-quality information.

2.3. Causal Evidence for Industrial Prediction

Causal learning is suitable for prediction variables that contain disturbance factors related to the labels in training but are not the actual causes. Reflection intensity may be associated with deformation in one dataset due to compression of samples at a particular station during photography. At different times of the day, they are not the same. Causal representation learning [17] seeks to mitigate the problem of unstable association by promoting the use of variables that remain meaningful after intervention or condition changes.

Industrial Prediction also needs audit trails. The reason for the result being a deformation warning should be specified as edge displacement, compression residual, load anomaly or poor image quality. Explainable quality-control research [18] shows that dominant-evidence output can help engineers decide whether to re-measure a sample, adjust the fixture or reject the product. Thus, causality-enhanced prediction is not only a model improvement but also aids in process diagnosis. Another problem is the lack of an engineering explanation for the statistics. A large feature contribution is not necessarily caused by a production problem; it may also be due to changes in light or focus of the camera. Causal inspection studies [19] show that the prediction evidence should remain consistent after reasonable alterations to the operation. Therefore, to some extent, causal regularisation will be employed instead of only attention scores.

Based on the above studies, the model of rubber-seal measurement needs to address problems of time, cross-source correlation and evidence reliability. State-Space Model has time-memory; Mixer block performs interactions among variables; Causal weight is a filter for unstable associations. Recent sequence-learning research [20] has also supported the use of both historical responses and current sensor quality for the target value.

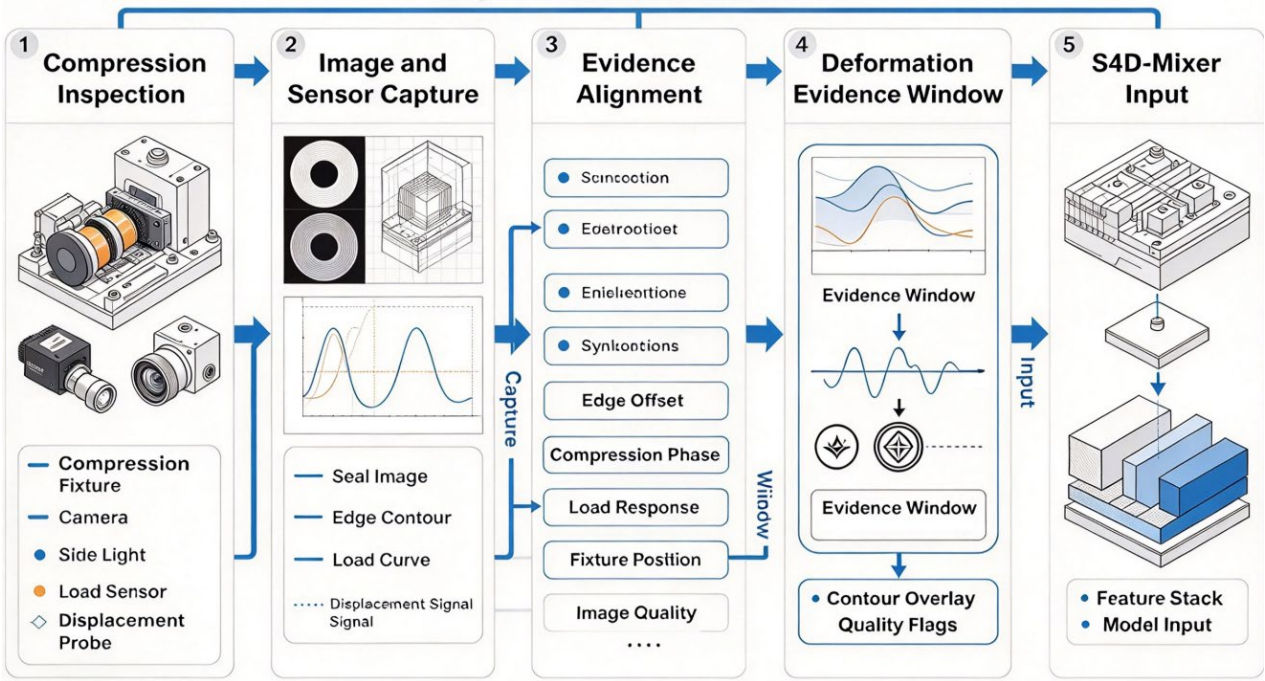


Figure 1. Rubber Seal Visual and Mechanical Evidence Representation Workflow

3. Methodology

3.1. Deformation Evidence Representation

The measurement window is based on a short production cycle. Seal image frames, extracted edge contours, compression displacement, applied load, fixture position and image quality are aligned within the same observation window. Figure 1 shows the workflow of rubber seal visual and mechanical evidence representation. the image-and-compression station provides edge displacement, load response and quality indicators that are aligned before load peak, during holding and after release. This design represents the deformation process rather than only the final contour.

The deformation state is represented by an aligned feature vector. It keeps visual and mechanical evidence in the same sampling window so that local edge movement can be compared with the applied compression condition.

$$x_t = [e_t, d_t, f_t, q_t, c_t] \tag{1}$$

In this expression, the variables describe edge offset, compression displacement, load response, image quality and fixture condition. The vector is a measurement state rather than a final quality label. It is used to preserve the observation context before prediction.

Edge deformation is calculated from the deviation between the observed contour and the nominal contour. The value is normalised by the nominal seal width so that different ring sizes can be compared under the same measurement scale.

$$r_t = \frac{|b_t - b_0|}{w_0} \tag{2}$$

The edge deviation is used to identify local compression, eccentric contact and folded regions. It is not sufficient alone because surface reflection or a partial contour loss can produce a similar edge offset. Mechanical evidence is therefore retained in the same window.

The measurement window is the phase of compression, and the same geometric deviation has different meanings at different times. The first deformation of the edge at the end of the loading is elastic; however, a displacement that occurs after the holding stage may be permanent. Therefore, the phase information will not be the same for all contour shifts in the model. It can also be linked to the fixture time for the prediction results and adjust the pressing speed or holding duration of the production line accordingly.

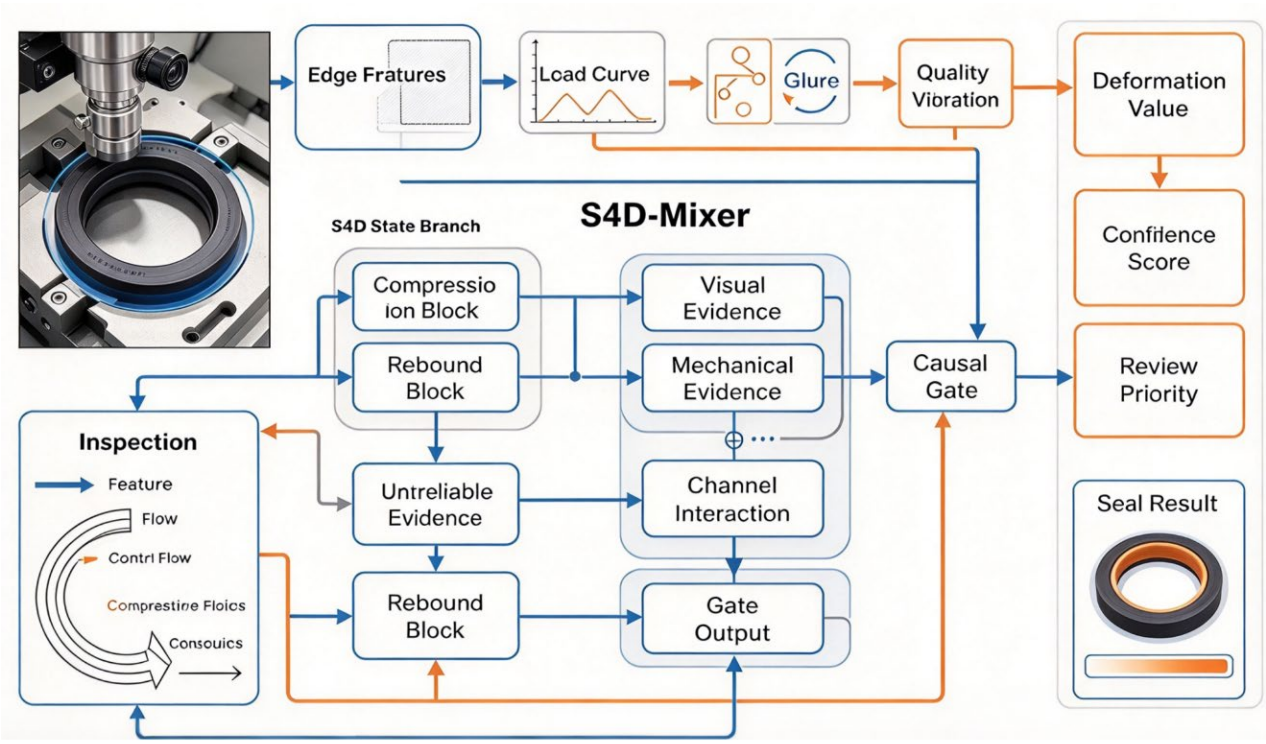


Figure 2. S4D-Mixer Backbone for Seal Deformation Prediction

3.2. S4D-Mixer Prediction Backbone

Figure 2 shows the S4D-Mixer backbone for seal deformation prediction. The left side receives seal image evidence, image-quality indicators and load-displacement curves. The S4D branch updates temporal deformation states across loading and recovery, while the Mixer branch coordinates channel interactions among visual and mechanical variables. The output branches provide predicted deformation, confidence and review priority. This architecture preserves process history while keeping the prediction auditable for production inspection.

The S4D branch uses a compact state update to model compression and rebound behaviour. It gives the model a memory of early deformation while avoiding the high computational cost of dense attention over all frames.

$$h_t = Ah_{t-1} + Bx_t \tag{3}$$

The hidden state stores the temporal deformation history. A stable loading period should update the state gently, while a sudden edge fold or load jump should produce a stronger update. This behaviour is important when deformation appears only for a short interval.

The state update is intentionally kept compact so that the model can be deployed in a production inspection station. A long image sequence may contain many repeated frames after the seal reaches stable compression. These frames should not dominate the representation. The S4D component keeps the earlier loading trend and later recovery trend in the same hidden state, so the model can compare whether the ring returns to the expected geometry after release.

The Mixer branch combines temporal states and channel variables. It allows visual and mechanical evidence to interact before the final deformation prediction is made.

$$z_t = W_2\sigma(W_1h_t) + Ux_t \tag{4}$$

The mixed feature is used to reduce dependence on a single observation source. For example, when an image is partially blurred, the displacement and load residual can still support the prediction. When load data fluctuate, the edge contour and image-quality variables can prevent overreaction.

The channel interaction is especially useful when one evidence source is temporarily weak. If the visual edge is interrupted by reflection, the compression load and displacement residual still provide mechanical continuity. If the load sensor has short vibration noise, the image contour and fixture position can constrain the prediction. The Mixer branch therefore works as an evidence coordinator rather than only a feature compressor.

The predicted deformation is obtained from the fused feature representation. A separate confidence branch uses the same evidence but is trained to reflect measurement reliability.

$$\hat{y}_t = W_yz_t + b_y \tag{5}$$

3.3. Causal Regularisation and Output Design

A causal factor is added to reduce unstable correlations. The model increases the influence of variables that remain consistent across compression conditions and reduces the influence of variables that change mainly because of lighting, fixture disturbance or temporary sensor weakness. The reliability index is relative to the current measurement condition rather than an inherent property of the sensor. This design is important because the same camera may provide strong edge evidence in one cycle and weak evidence in another cycle because of surface reflection.

$$\alpha_i = \mathrm{softmax}(s_ig_i) \tag{6}$$

The causal weight links the statistical contribution with the physical reliability score. A high contribution is not accepted as useful evidence if the variable has low physical reliability under the current measurement condition.

The final optimisation combines deformation error, causal regularisation and confidence calibration. The objective is short enough to keep the formulation readable while still representing the three functions required by the model.

$$L = L_y + \lambda_1L_c + \lambda_2L_u \tag{7}$$

The first term controls deformation accuracy, the second term suppresses unstable evidence, and the third term calibrates confidence. The output contains predicted deformation, confidence score, dominant evidence and review priority. This structure allows the inspection system to distinguish a reliable deformation alarm from a sample requiring remeasurement.

The prediction output is designed for a quality-inspection workflow. The deformation value supports tolerance checking, the confidence score supports remeasurement decisions, and dominant evidence supports process diagnosis. The output therefore avoids using a single regression value as the only basis for production decisions. Station-level

logs can also store deformation value, confidence and evidence source so that repeated warnings from the same mould cavity, camera station or compression fixture can be reviewed later.

4. Results and Discussion

4.1. Dataset Construction and Measurement Conditions

The 5,280 simulated measurement windows cover normal compression, under-compression, over-compression, eccentric compression and edge-folded states [21]. Figure 3 presents sample composition and measurement conditions. Figure 3(a) shows state distribution, where normal compression is more frequent and edge-folded states are less frequent to reflect production imbalance. Figure 3(b) shows deformation amplitude, where eccentric compression has a larger deviation than normal under-compression. Figure 3(c) shows image-quality variation, where reflective rubber surfaces produce a low-quality tail. Figure 3(d) shows load-stability distribution, where some high-deformation samples also include fixture disturbance.

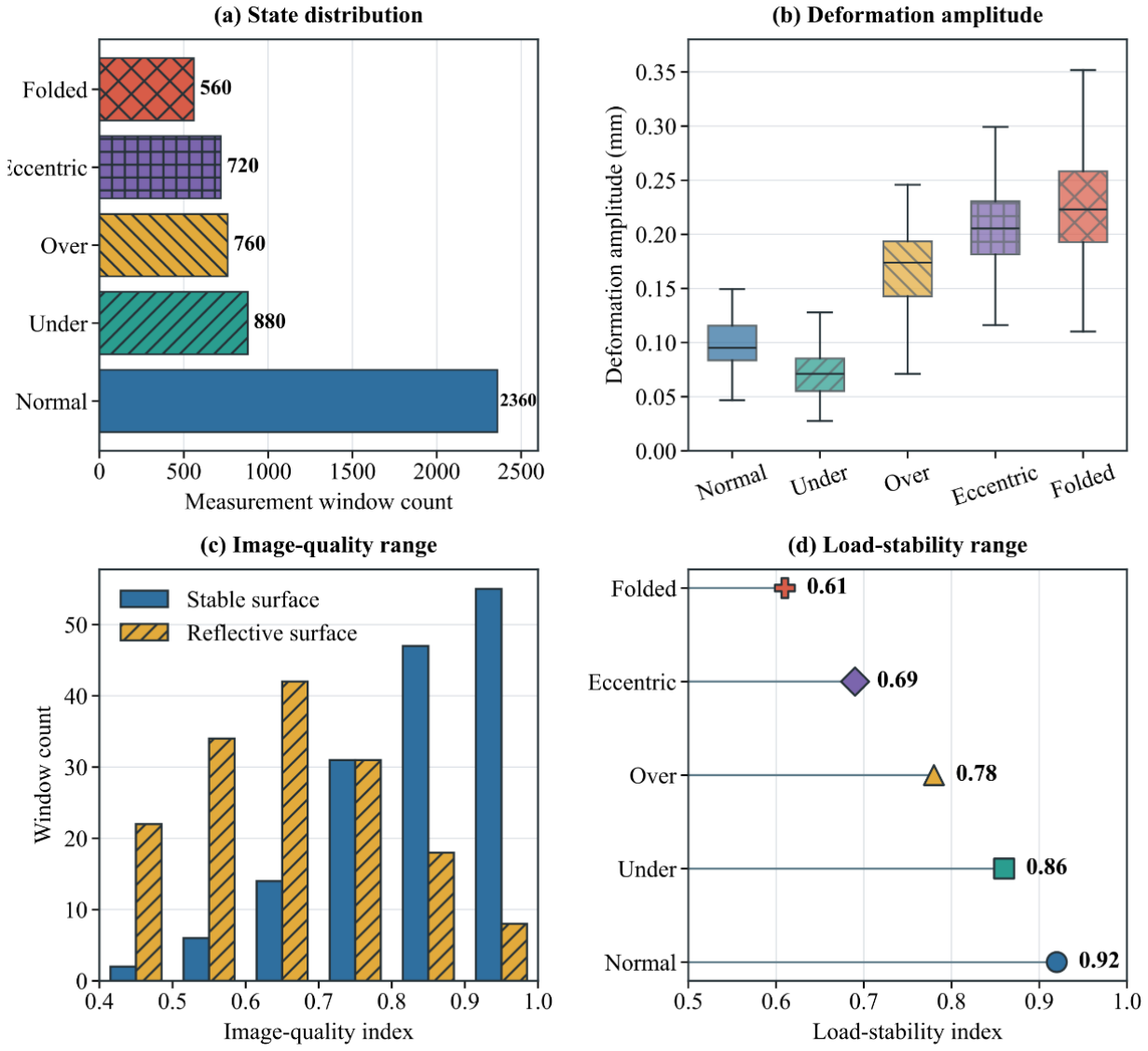


Figure 3. Seal sample and deformation distribution. (a) State distribution. (b) Deformation amplitude. (c) Image-quality range. (d) Load-stability range.

The dataset is used to quantify deformation rather than to perform random defect classification. Measurement datasets for flexible components [22] should include ambiguous samples because acceptable elastic compression and premature failure may be separated by a gradual boundary. Each sample therefore contains continuous deformation data and an engineering label. This structure prevents the model from learning only a binary pass-fail rule and makes it more relevant to production decisions involving remeasurement or rejection.

The uneven distribution of deformation states is retained to match production conditions. Most seals are normal, whereas serious folds and eccentric compressions are rare. Imbalanced industrial evaluation studies [23] show that

artificially balanced datasets can overestimate deployment performance. Therefore, mean error, recall, confidence and review priority are evaluated together. This choice reduces false alarms for normal seals while preserving sensitivity to rare deformation states that may cause leakage or premature failure.

Figure 4 shows the relationship between load-displacement response and image-quality variation. Figure 4(a) shows that over-compressed rings have a higher load increase than normal rings at the same displacement. Figure 4(b) shows that low-quality images affect edge localization more severely than load response. Recent rubber-component inspection work [24] also indicates that automated inspection should evaluate image and mechanical evidence together. A delayed force increase with a stable contour may indicate material stiffness variation, while sudden contour change without load increase may indicate imaging or fixture error.

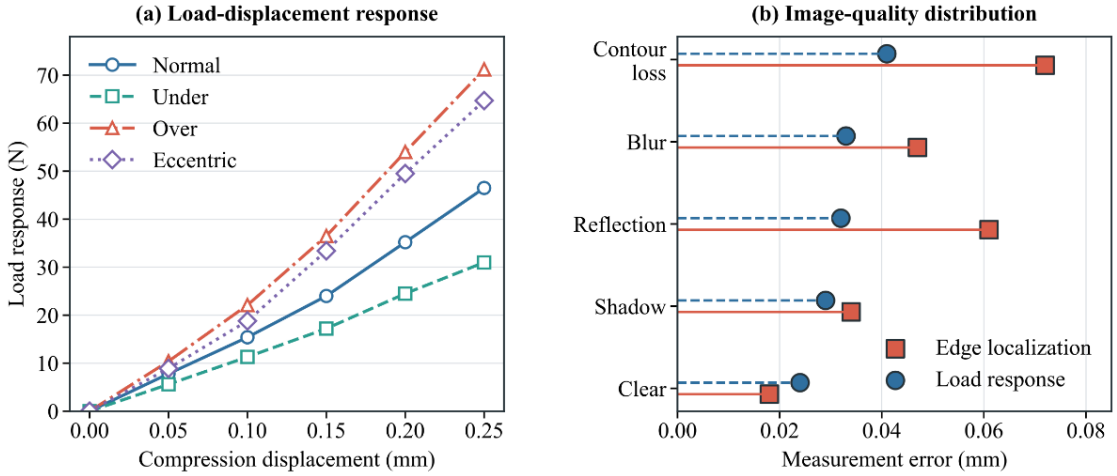


Figure 4. Load-displacement and image-quality variation. (a) Load-displacement response. (b) Image-quality distribution.

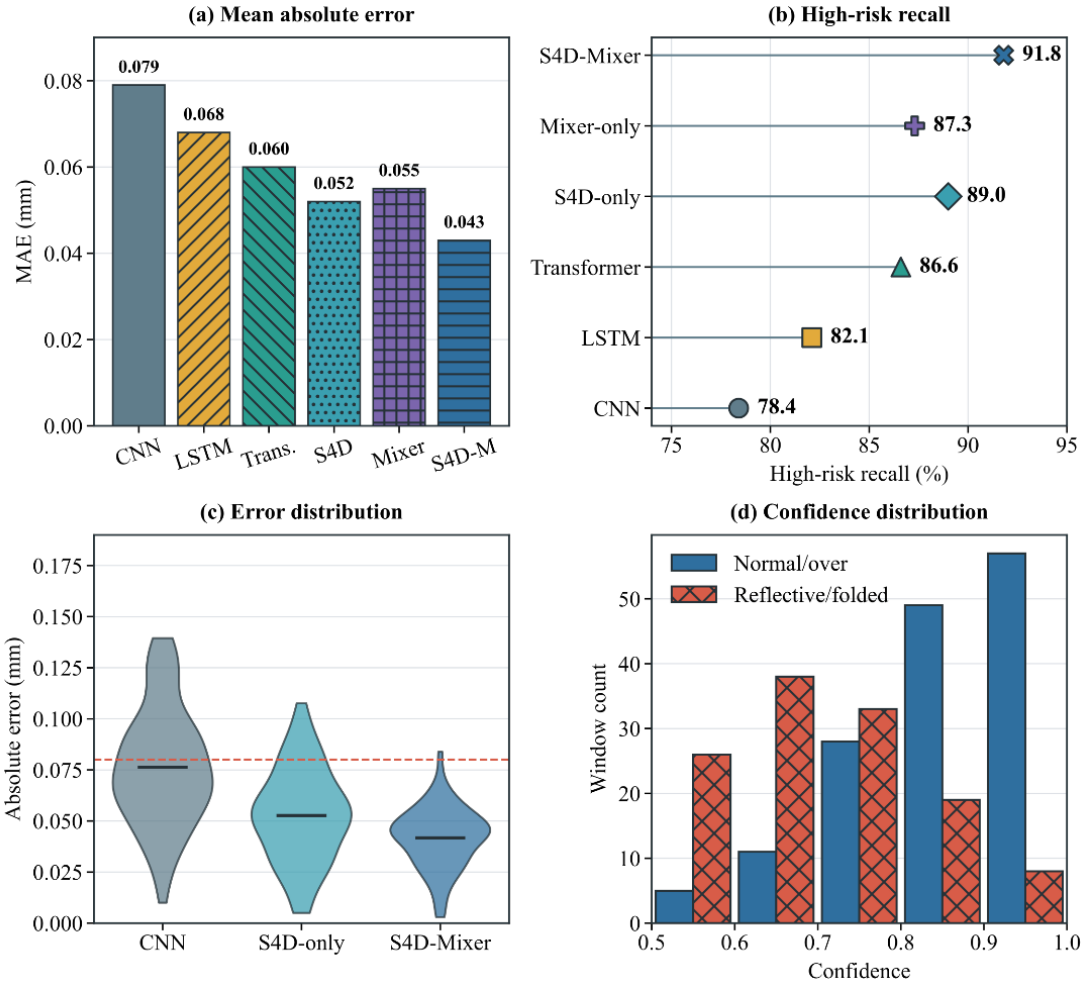


Figure 5. Baseline comparison and measurement error. (a) Mean absolute error. (b) High-risk recall. (c) Error distribution. (d) Confidence distribution.

4.2. rediction Accuracy and Generalisation

The new model is compared with CNN, LSTM, Transformer, S4D-only and Mixer-only baselines [25]. Figure 5 presents baseline comparison and measurement error distribution. Figure 5(a) reports a mean absolute error of 0.043 mm for the proposed model. Figure 5(b) reports 91.8% high-risk deformation recall, exceeding the S4D-only model. Figure 5(c) shows that most errors remain within the process tolerance limit. Figure 5(d) shows that low-confidence cases mainly come from reflective and edge-folded samples. These results indicate that temporal features and causal weighting reduce unstable measurement errors.

Table 1 shows the quantitative results of different seal conditions. Since both over-compression and eccentric compression are considered uniform load and contour-variation problems, the model is more suitable for these types of problems. Edge-folded samples are even harder to obtain, and the fold may be uneven or partially hidden by the camera. Similar behaviour has been reported in quality prediction studies [26], and rare local defects are even more difficult than global deformation trends. Therefore, a table can be used to show the confidence values; not all measurements are equally reliable. The values show that the model is not always very confident in all of the cases. Normal compression and excessive compression have different mechanical properties, and edge-folded states are more locally visually ambiguous. According to the experience of engineering practice, the local folds are caused by angles, shadows and partial occlusions. Therefore, according to the confidence level of the model's output, it should not be considered the precise value.

Table 1. Prediction accuracy under different seal conditions.

Condition	MAE (mm)	RMSE (mm)	Recall (%)	Confidence
Normal compression	0.031	0.044	94.2	0.93
Under-compression	0.046	0.061	90.5	0.88
Over-compression	0.039	0.053	93.1	0.91
Eccentric compression	0.052	0.069	89.7	0.86
Edge-folded state	0.061	0.081	85.6	0.79

Figure 6 shows generalisation under unseen deformation conditions. Figure 6(a) presents fixture-offset disturbance, where the ring is not physically deformed but its observed position changes. The causal branch reduces the weight of unstable fixture variables and therefore decreases false alarms. Figure 6(b) presents unseen compression depth, where the proposed model produces a smoother error curve than the Transformer baseline. Generalisable industrial inspection research [27] indicates that condition shift should be evaluated rather than relying only on random sample splitting.

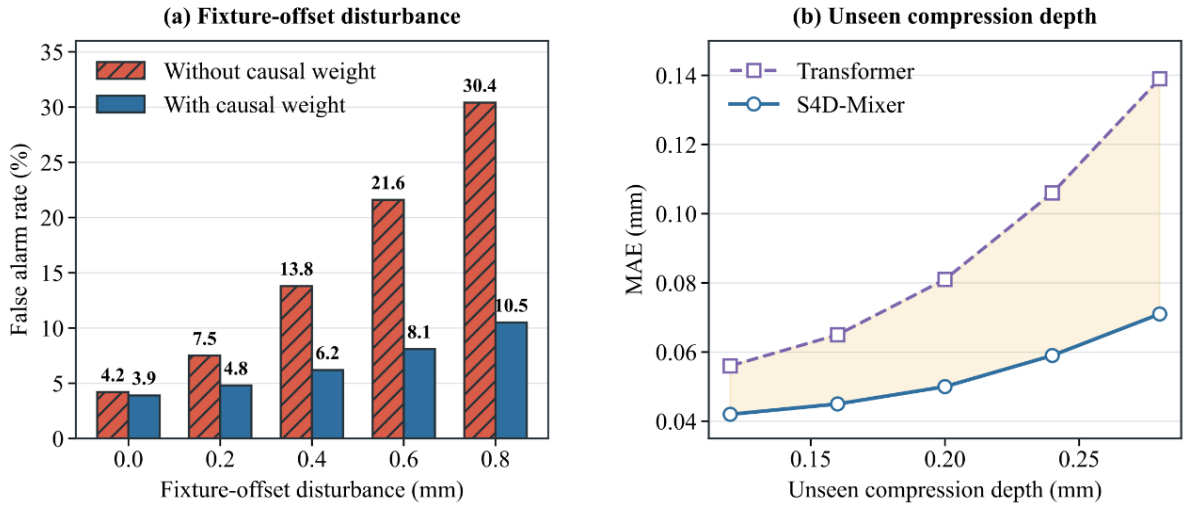


Figure 6. Generalisation under unseen deformation conditions. (a) Fixture-offset disturbance. (b) Unseen compression depth.

It is also qualitative in nature. A typical CNN can find a prominent alteration in shape, but it will fail to recognise a delayed rebound deformation. LSTM can handle the order of time, but it is not very effective in dealing with visual quality and load reduction. Transformer attention can learn long-distance dependencies; however, it is also affected by irrelevant static frames. State-Space models [28] are suitable for long sequences, and a mixer branch improves cross-variable interaction. Therefore, the proposed Design is closer to the actual process of seal compression than a single-source model. The results also show that a stable process model should conform to the physics of compression. At the

actual station, there is no individual check of the seals; instead, they are grouped together and then pressed, held and released by a controlled displacement. The first purpose of the model proposed above is to preserve the temporal relationship and determine whether the visual deformation is due to mechanical changes. As shown in the comparison, the proposed model is also not based on a single type of feature. Stable visual information can help the image branch locate the edge reliably. In the absence of visual evidence, the model will not output an unsupported deformation estimate for mechanical variables. This behaviour is required for a practical inspection station because the imaging conditions of the rubber surface vary in different batches.

Generalisation results also show that the causal module is less sensitive to station-specific features. Slight camera displacement changes the image position of the curve but not the mechanical deformation process, so a model without causal weighting may incorrectly attribute the shift to deformation. Reliability-aware fusion research [29] assigns different trust levels to sources under disturbance. The proposed model uses load-displacement consistency and image-quality evidence to reject unstable visual correlations that may arise from fixture wear, surface dirt or camera drift.

4.3. Causal Evidence and Engineering Use

Figure 7 shows causal evidence ranking and confidence output. Figure 7(a) presents edge-offset contribution for normal visual deformation cases. Figure 7(b) shows that load residual is dominant during over-compression. Figure 7(c) shows that image-quality uncertainty is high for reflective rubber surfaces. Figure 7(d) presents review-priority output, where low-confidence high-deformation samples are routed to remeasurement rather than immediate rejection. Explainable inspection research [30] supports this type of evidence ranking because it converts a prediction into an auditable engineering decision.

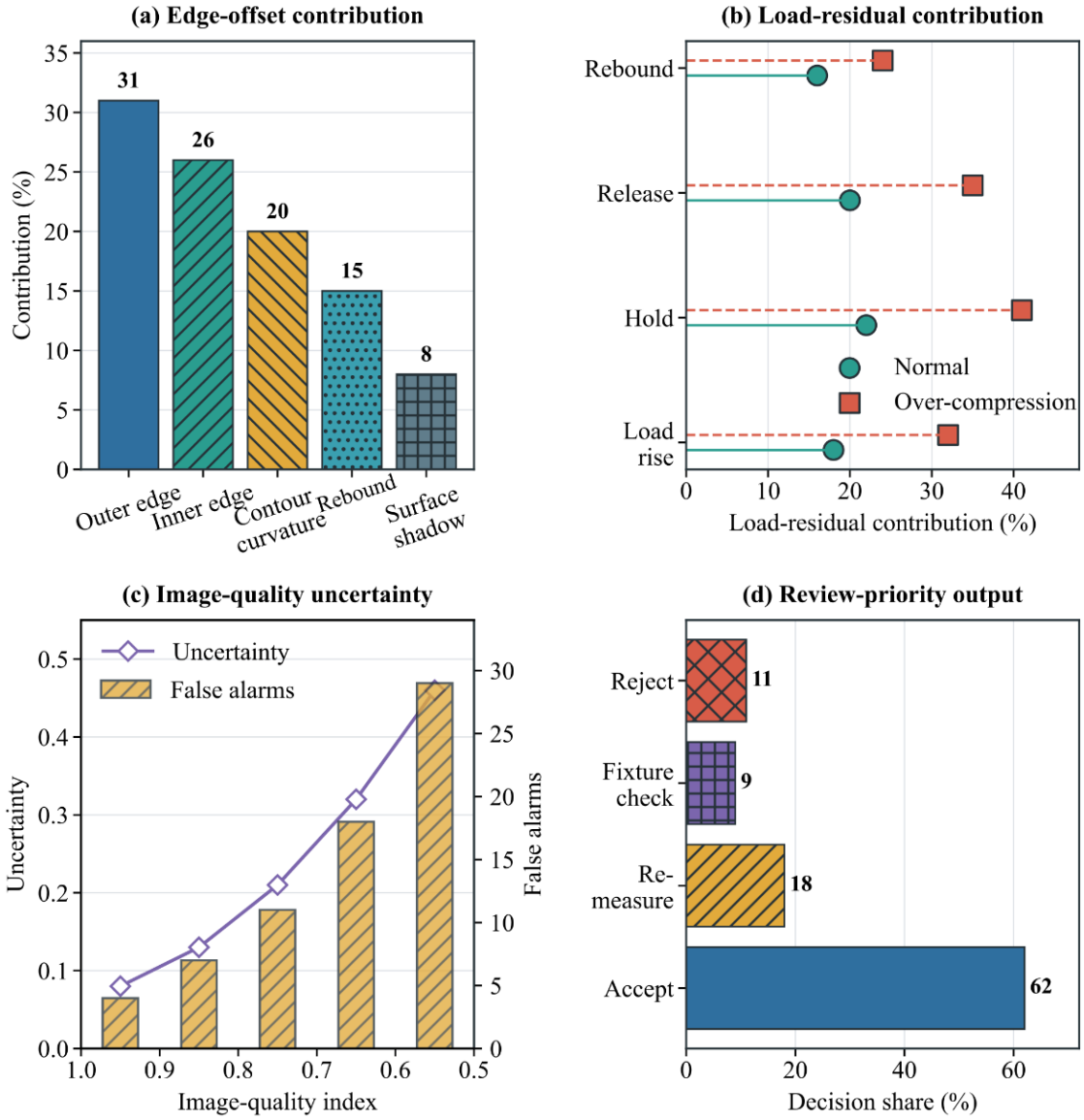


Figure 7. Causal evidence ranking and confidence output. (a) Edge-offset contribution. (b) Load-residual contribution. (c) Image-quality uncertainty. (d) Review-priority output.

The causal module explains why the model avoids certain false alarms. A conventional edge detector may produce a distorted contour from mirror-like reflection under normal mechanical load. The causal weight reduces the influence of this edge feature when image quality is low and load response is stable. Reliable multimodal fusion research [31] indicates that reliable evidence weighting can prevent a single weak source from dominating the result. This distinction helps engineers separate measurement uncertainty from actual component risk.

Causal evidence output can also support process diagnosis. High edge-offset contribution with low load residual may indicate visual contour disturbance or a local surface mark, whereas large load residual with stable image edges may indicate fixture displacement or force-control drift. Industrial decision-support studies [32] show that separated evidence helps engineers choose follow-up actions without treating every warning as a product defect. The review log can therefore be used to distinguish material variation from measurement-system drift.

Figure 8 presents inspection decision and review-priority output. Figure 8(a) shows predicted deformation and the acceptance or rejection decision. Figure 8(b) shows the review record structure, including deformation value, confidence and dominant evidence. Predictive maintenance studies [33] indicate that traceable quality records can help correct process drift. The decision output does not replace the process engineer; instead, high-confidence severe deformation can be rejected, while high deformation with low confidence should trigger remeasurement before a final decision.

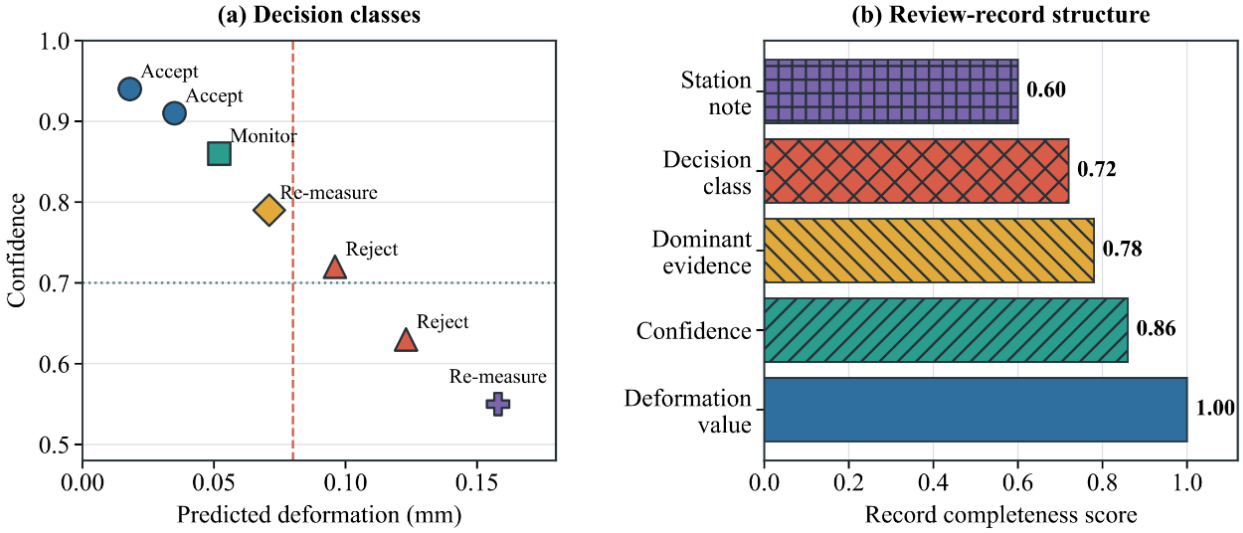


Figure 8. Inspection decision and review-priority output. (a) Decision classes. (b) Review-record structure.

The review records can support continuous improvement. Repeated low-confidence results in the same camera area may indicate lighting misalignment, whereas repeated eccentric-compression warnings may indicate fixture wear. Production learning research [34] supports linking inspection data with subsequent process feedback. The model output therefore connects part-level measurement with station-level maintenance and calibration planning.

The module structure of the proposed output is suitable for industrial use because it separates measurement, confidence and action. High-confidence over-compression can support immediate rejection, while a low-confidence edge-fold warning should request remeasurement. Industrial deployment research [35] indicates that quality models should be monitored for gradual performance decline after installation. Review-priority output can collect uncertain samples for calibration without stopping the entire production line, while high-confidence risk samples remain available for direct replacement or rejection.

5. Conclusion

This study presented a causality-enhanced S4D-Mixer model for rubber seal deformation measurement, and the overall conclusion is that visual contour evidence, load-displacement response, recovery behavior and measurement reliability should be evaluated jointly for traceable seal inspection. First, simulated results show that the proposed model achieves a mean absolute deformation error of 0.043 mm and 91.8% high-risk deformation recall, indicating that temporal modelling and causal weighting improve measurement reliability. Second, the comparative results show that over-compression and eccentric compression are better characterized when edge and load evidence are considered together, while edge-folded cases remain more difficult because of local visual ambiguity. Third, the main limitation is that the evaluation relies on simulated production windows and simplified material conditions; therefore, future validation should include factory data across rubber lots, temperatures, light-exposure conditions, assembly equipment and off-line remeasurement records.

The proposed output separates predicted deformation, confidence, dominant evidence and review priority. This structure supports reliable rejection for high-confidence severe deformation, remeasurement for low-confidence high-deformation samples and station maintenance review when repeated warnings point to fixture or imaging problems. Causal evidence ranking helps determine whether a warning is mainly associated with edge offset, load residual, image quality or fixture condition, which is necessary for traceable process diagnosis.

Future work should acquire extended factory data covering rubber lots, temperature variation, light exposure, assembly equipment and calibrated off-line measurements. Additional validation should include material ageing, oil contamination, extended compression set and storage-condition effects because these factors may alter the relationship between load response and visible deformation. The review records generated by the model can serve as calibration samples for updating thresholds and maintaining long-term inspection reliability.

6. Declarations

6.1. Author Contributions

Dimas Firmansyah contributes to conceptualization, methodology, software, validation, analysis, investigation, data collection, draft preparation, manuscript editing, visualization, supervision, project administration, and funding acquisition. Luthfi Ramadhan contributes to validation, analysis, investigation, data collection, draft preparation. All authors have read and agreed with the manuscript before its submission and publication.

6.2. Funding and Acknowledgments

This research received no specific financial support from any funding agency.

6.3. Institutional Review Board Statement

Not applicable.

6.4. Informed Consent Statement

Not applicable.

6.5. Data Availability

Not applicable.

6.6. Declaration of Competing Interest

The authors declare that they have no known competing financial interests or personal relationships that could have appeared to influence the work reported in this paper.

6.7. Declaration of generative AI and AI-assisted technologies

During the preparation of this manuscript, the authors utilized Grammarly for linguistic polishing, logical organization and draft revision. The generative AI tool was not involved in research design, data collection, data analysis, or the equation of core conclusions. All outputs generated by AI were reviewed, revised and verified manually by the authors. The authors take full responsibility for all content of this manuscript.

7. References

[1] Zong, Y., Liu, T., Ren, L., & Bao, G. (2024). Research on the friction force characteristics for the double O-ring seal of the cylinder under the small displacement condition. Tribology Transactions, 67(6), 1273–1281. https://doi.org/10.1080/10402004.2024.2422420

[2] Yu, S., He, X., & Zhu, C. (2024). Three-dimension deformation measurement using modified microscopic stereo-vision technology. Measurement, 228, 114291. https://doi.org/10.1016/j.measurement.2024.114291

[3] Shiney, S. A., Seetharaman, R., Sharmila, V. J., & Prathiba, S. (2025). Deep learning-based gasket fault detection: A CNN approach. Scientific Reports, 15, 4776. https://doi.org/10.1038/s41598-025-85223-8

[4] Jin, L., & Che, L. (2024). Experimental study on stress relaxation of rubber O-ring for mechanical seal. Journal of Physics: Conference Series, 2691(1), 012015. https://doi.org/10.1088/1742-6596/2691/1/012015

[5] Hütten, N., Alves Gomes, M., Hölken, F., Andricevic, K., Meyes, R., & Meisen, T. (2024). Deep learning for automated visual inspection in manufacturing and maintenance: A survey of open-access papers. Applied System Innovation, 7(1), 11. https://doi.org/10.3390/asi7010011

[6] Tiezzi, M., Casoni, M., Betti, A., Gori, M., & Melacci, S. (2026). State-space modeling in long sequence processing: A survey on recurrence in the transformer era. Neural Networks, 193, 108039. https://doi.org/10.1016/j.neunet.2025.108039

[7] Fu, Y., & Lu, J. (2026). SFR-Mixer: Scale-fusion residual mixer for long-term multivariate time-series forecasting correction. IEEE Access, 14, 146424–146434. https://doi.org/10.1109/access.2026.3735532

[8] Feng, Z., Dong, C., Xu, X., Liu, Y., & Wang, S. (2024). Deep learning-based automated optical inspection system for the additive manufacturing of diamond tools. 3D Printing and Additive Manufacturing, 11(6), e2045–e2060. https://doi.org/10.1089/3dp.2023.0208

[9] Wang, C., Wei, X., & Jiang, X. (2024). An automated defect detection method for optimizing industrial quality inspection. Engineering Applications of Artificial Intelligence, 127, 107387. https://doi.org/10.1016/j.engappai.2023.107387

[10] Rožanec, J. M., Bizjak, L., Trajkova, E., Zajec, P., Keizer, J., Fortuna, B., & Mladenić, D. (2024). Active learning and novel model calibration measurements for automated visual inspection in manufacturing. Journal of Intelligent Manufacturing, 35(5), 1963–1984. https://doi.org/10.1007/s10845-023-02098-0

[11] Zhou, W., & Xie, Z. (2025). Sealing rubber ring design based on machine learning algorithm combined progressive optimization method. Tribology International, 201, 110173. https://doi.org/10.1016/j.triboint.2024.110173

[12] Ameri, R., Hsu, C. C., & Band, S. S. (2024). A systematic review of deep learning approaches for surface defect detection in industrial applications. Engineering Applications of Artificial Intelligence, 130, 107717. https://doi.org/10.1016/j.engappai.2023.107717

[13] Poyraz, A. G., Kaçmaz, M., Gürkan, H., & Dirik, A. E. (2024). Sub-pixel counting based diameter measurement algorithm for industrial machine vision. Measurement, 225, 114063. https://doi.org/10.1016/j.measurement.2023.114063

[14] Patro, B. N., & Agneeswaran, V. S. (2025). Mamba-360: Survey of state space models as transformer alternative for long sequence modelling: Methods, applications, and challenges. Engineering Applications of Artificial Intelligence, 159, 111279. https://doi.org/10.1016/j.engappai.2025.111279

[15] Bulgakov, G., Rudenko, D., Molodtsov, G., & Beznosikov, A. (2026). Bridging KANs and tabular deep learning: Feature embeddings and efficient ensembling. IEEE Access, 14, 30073–30086. https://doi.org/10.1109/access.2026.3663928

[16] Oliveira, R. M. A., Sant'Anna, Â. M. O., & da Silva, P. H. F. (2024). Explainable machine learning models for defects detection in industrial processes. Computers & Industrial Engineering, 192, 110214. https://doi.org/10.1016/j.cie.2024.110214

[17] Karimi Mamaghan, A. M., Dittadi, A., Bauer, S., Johansson, K. H., & Quinzan, F. (2024). Diffusion-based causal representation learning. Entropy, 26(7), 556. https://doi.org/10.3390/e26070556

[18] Rožanec, J. M., Šircelj, B., Fortuna, B., & Mladenić, D. (2024). Adaptive explainable artificial intelligence for visual defect inspection. Procedia Computer Science, 232, 3034–3043. https://doi.org/10.1016/j.procs.2024.02.119

[19] Chen, M., Wang, H., Wang, R., Peng, Y., & Zhang, H. (2024). CDRM: Causal disentangled representation learning for missing data. Knowledge-Based Systems, 299, 112079. https://doi.org/10.1016/j.knosys.2024.112079

[20] Zhang, Z., Tian, G., Guo, F., & Wang, P. (2025). TFP-mixer: A lightweight time and frequency combining model for multivariate long-term time series forecasting. Applied Intelligence, 55(10), 695. https://doi.org/10.1007/s10489-025-06562-7

[21] Lara-Chávez, J. A., Avilés-Cruz, C., & Magos-Rivera, M. (2026). Deep learning model for automated visual inspection of electronic boards. Journal of Intelligent Manufacturing, 37(11), 4801–4819. https://doi.org/10.1007/s10845-025-02748-5

[22] Ma, Y., Yin, J., Huang, F., & Li, Q. (2024). Surface defect inspection of industrial products with object detection deep networks: A systematic review. Artificial Intelligence Review, 57(12), 333. https://doi.org/10.1007/s10462-024-10956-3

[23] Kim, H., Kim, D., Ahn, P., Suh, S., Cho, H., & Kim, J. (2024). ContextMix: A context-aware data augmentation method for industrial visual inspection systems. Engineering Applications of Artificial Intelligence, 131, 107842. https://doi.org/10.1016/j.engappai.2023.107842

[24] Cheng, W., Gao, F., Li, Y., Zhang, H., Li, W., & Wu, K. (2025). A machine vision-based dimension measurement method of shaft parts with sub-pixel edge. Measurement Science and Technology, 36(5), 055026. https://doi.org/10.1088/1361-6501/adcc47

[25] Jayawardena, A., Sul, J. H., Moratuwage, D., Wijayaraja, J. L., & Piyathilaka, L. (2026). State of the art in AI-based visual inspection for industrial quality control: Methods, benchmarks, challenges, and autonomous systems. Electronics, 15(12), 2727. https://doi.org/10.3390/electronics15122727

[26] El Wahabi, A., Mesquiny, A., El Ahmadi, O., Baraka, I. H., Hamdoune, S., & Boudhir, A. A. (2025). Enhancing quality inspection in automotive manufacturing through deep learning and transfer learning. Neural Computing and Applications, 37(18), 11711–11736. https://doi.org/10.1007/s00521-024-10534-2

[27] Lara, M. A., Hameed, I. A., & Koziorek, J. (2025). Anomaly-focused augmentation method for industrial visual inspection. IEEE Access, 13, 89118–89139. https://doi.org/10.1109/access.2025.3570075

[28] Özçelik, R., de Ruiter, S., Criscuolo, E., & Grisoni, F. (2024). Chemical language modeling with structured state space sequence models. Nature Communications, 15, 6176. https://doi.org/10.1038/s41467-024-50469-9

[29] Rajkumar, S. C., & Yuvasini, D. (2026). Reliability-aware adaptive multimodal fusion framework for robust continuous authentication under non-stationary sensing conditions. Pattern Analysis and Applications, 29(3), 154. https://doi.org/10.1007/s10044-026-01739-3

[30] Bitterling, C., Loske, D., & Klumpp, M. (2025). Improving visual inspection accuracy: Explainable AI for human-centric quality control. IFAC-PapersOnLine, 59(10), 1450–1455. https://doi.org/10.1016/j.ifacol.2025.09.244

[31] Wang, J., Niu, Y., & Huang, B. (2025). Fusion-restoration model for industrial multimodal anomaly detection. Neurocomputing, 637, 130073. https://doi.org/10.1016/j.neucom.2025.130073

[32] Hoang, D. C., Tan, P. X., Nguyen, A. N., Duong, T. H. A., Huynh, T. M., Nguyen, D. M., Cao, M. D., Ngo, D. H., Nguyen, T. U., Phan, K. T., Do, M. Q., Dinh, X. T., Duong, V. H., Hoang, N. A., & Nguyen, V. T. (2025). Accurate industrial anomaly detection with efficient multimodal fusion. Array, 28, 100512. https://doi.org/10.1016/j.array.2025.100512

[33] AL-Ali, M., & Alharbi, A. (2026). Temporally rigorous and traceable predictive maintenance via joint labeler-model optimization. Scientific Reports, 16, 22583. https://doi.org/10.1038/s41598-026-52210-6

[34] Prieto, R. S., Bravo Montenegro, D. A., & Rengifo, C. (2024). Machine hearing for predictive maintenance of BLDC motors. Journal of Quality in Maintenance Engineering, 30(3), 540–561. https://doi.org/10.1108/jqme-12-2023-0115

[35] Wang, Y., Yuan, H., Zhang, M., Li, H., & Li, Y. (2026). Industrial inspection system based on multimodal data fusion. IEEE Sensors Journal, 26(5), 7579–7594. https://doi.org/10.1109/jsen.2026.3652614